

# Supporting Information for:

## Integrating the evidence for a terrestrial carbon sink caused by increasing atmospheric CO<sub>2</sub>

Anthony P. Walker, Martin G. De Kauwe, Ana Bastos, Soumaya Belmecheri, Katerina Georgiou, Ralph Keeling, Sean M. McMahon, Belinda E. Medlyn, David J. P. Moore, Richard J. Norby, Sönke Zaehle, Kristina J. Anderson-Teixeira, Giovanna Battipaglia, Roel J. W. Brienen, Kristine G. Cabugao, Maxime Cailleret, Elliott Campbell, Josep Canadell, Philippe Ciais, Matthew E. Craig, David Ellsworth, Graham Farquhar, Simone Fatichi, Joshua B. Fisher, David Frank, Heather Graven, Lianhong Gu, Vanessa Haverd, Kelly Heilman, Martin Heimann, Bruce A. Hungate, Colleen M. Iversen, Fortunat Joos, Mingkai Jiang, Trevor F. Keenan, Jürgen Knauer, Christian Körner, Victor O. Leshyk, Sebastian Leuzinger, Yao Liu, Natasha MacBean, Yadvinder Malhi, Tim McVicar, Josep Penuelas, Julia Pongratz, A. Shafer Powell, Terhi Riutta, Manon E. B. Sabot, Juergen Schleucher, Stephen Sitch, William K. Smith, Benjamin Sulman, Benton Taylor, César Terrer, Margaret S. Torn, Kathleen Treseder, Anna T. Trugman, Susan E. Trumbore, Phillip J. van Mantgem, Steve L. Voelker, Mary E. Whelan, Pieter A. Zuidema

Article acceptance date: 6<sup>th</sup> July 2020.

## Notes S1. Standardising CO<sub>2</sub> responses with a $\beta$ factor

In order to compare across studies that measure different variables at different CO<sub>2</sub> concentrations and at different periods in time, we calculate a standardised CO<sub>2</sub> response metric. This metric is often referred to as the  $\beta$  factor (Friedlingstein et al., 1995; Bacastow and Keeling 1973). Multiple methods have been proposed and here we explore just a few to make an informed choice on the method to calculate  $\beta$  that best suits our purposes and so that the reader can visualise how  $\beta$  relates to different CO<sub>2</sub> response scenarios across a range of realistic CO<sub>2</sub> concentrations. We investigated three methods to calculate  $\beta$ , the normalised response ratio:

$$\beta = (rr_y - 1) / (rr_{CO_2} - 1), \quad (\text{Eq. S1})$$

log- $\beta$  (Bacastow and Keeling 1973):

$$\beta_{\log} = (rr_y - 1) / \ln(rr_{CO_2}), \quad (\text{Eq. S2})$$

and log-log- $\beta$ :

$$\beta_{\log-\log} = \ln(rr_y) / \ln(rr_{CO_2}), \quad (\text{Eq. S3})$$

where  $rr_y = y_e/y_a$  and  $rr_{CO_2} = CO_{2,e}/CO_{2,a}$ .  $y_a$  and  $y_e$  are the value of any response variable at low CO<sub>2</sub> and higher CO<sub>2</sub>, and  $CO_{2,a}$  and  $CO_{2,e}$  are the CO<sub>2</sub> concentrations.

Figure S1 shows the value of the two variations of the  $\beta$ -factors under different CO<sub>2</sub> response scenarios. As is clear from these figures  $\beta_{\log-\log}$  provides the most consistent characterisation of the CO<sub>2</sub> response.  $\beta_{\log-\log}$  is independent of the magnitude of the change in CO<sub>2</sub> (Figure S1), and also has a value of 1 when  $y$  is proportional to CO<sub>2</sub> (and thus  $rr_y$  is directly proportional to  $rr_{CO_2}$  which is important to identify to evaluate theory, see Section 2.1). We therefore choose  $\beta_{\log-\log}$  as our standardised CO<sub>2</sub> response metric.

Calculation of uncertainty in  $\beta_{\log-\log}$  is by error propagation:

$$\sigma_{f(x)} = f(x) \cdot ( (\sigma_{x1}/x_1)^2 + (\sigma_{x2}/x_2)^2 \dots + (\sigma_{xn}/x_n)^2 )^{0.5} \quad (\text{Eq. S4})$$

$$\sigma_{\ln(x)} = \sigma_x / x \quad (\text{Eq. S5})$$

where  $f(x)$  is a function of the vector  $x$  that combines the elements of  $x$  through multiplication or division,  $\sigma_x$  is a vector of the uncertainty in  $x$ , and  $\sigma_{\ln(x)}$  is the uncertainty in the scalar  $\ln(x)$ .

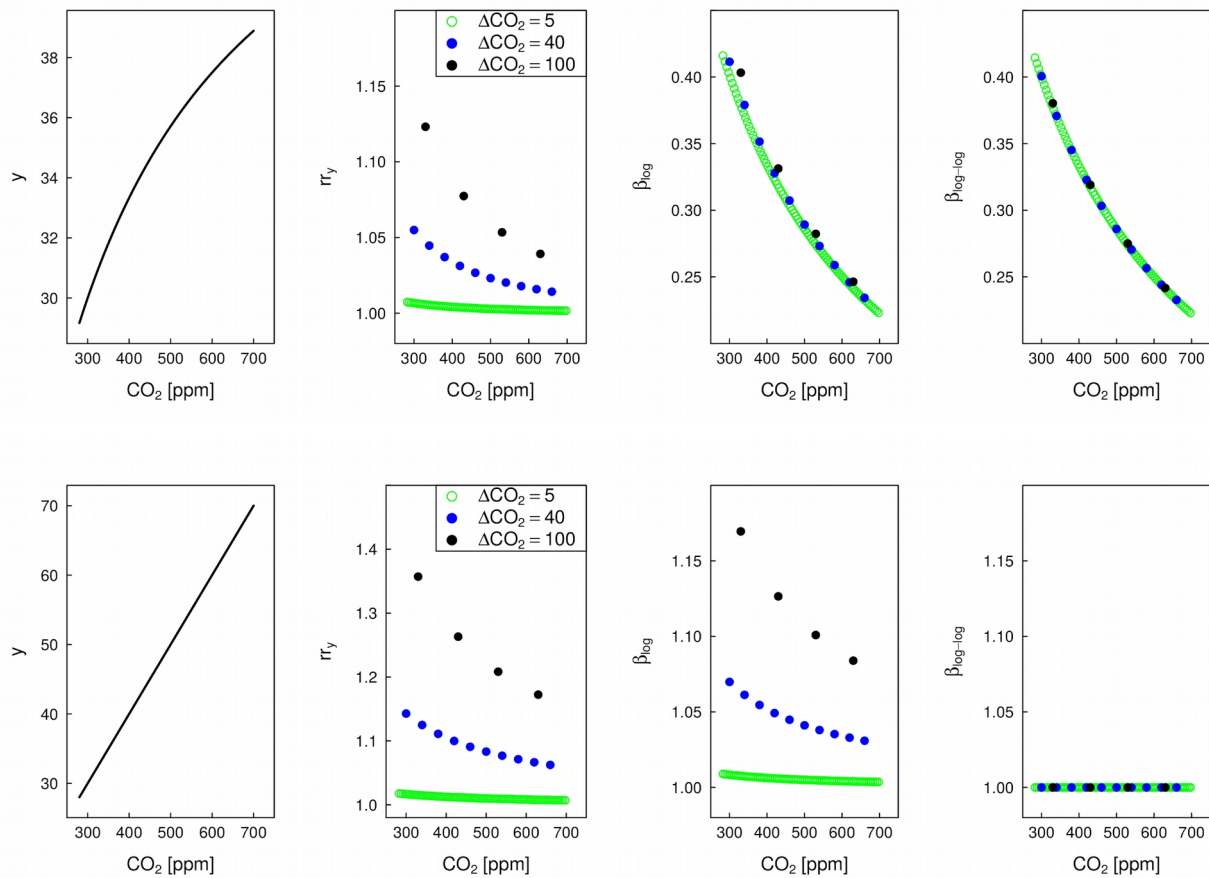


Figure S1. Calculation of response ratio ( $rr_y$ , column second from left),  $\beta_{\log}$  (Eq. S2, column third from left), and  $\beta_{\log-\log}$  (Eq. S3, right column) from theoretical CO<sub>2</sub> responses of an arbitrary variable ( $y$ , left column) that responds to CO<sub>2</sub> in proportion (lower row) or as a saturating function (upper row). Three different magnitudes of the change in CO<sub>2</sub> are used to calculate the response ratio and  $\beta$ s, 5 ppm (green), 40 ppm (blue), and 100 ppm (black).

## Notes S2. Calculation of $\beta$ from different data types

For time-series that use regression to infer trends we use the y-value of the regression for the first year of data and the last year of data (for  $y_a$  and  $y_e$ ). Where regressions were not given we use means of the first and last five years of the data to calculate  $x$  and  $\text{CO}_2$ . Where response variables were presented per year or per ppm we calculated the full change over the time period by multiplying by the length of, or by the change in  $\text{CO}_2$  over, the time period of the data used in the study. Where studies presented only an absolute change, where possible we calculated  $x_a$  from a mean value ( $x_t$ ) recorded at time  $t$  by subtracting the cumulative change up until time  $t$ . We then calculated  $x_e$  from  $x_a$  plus the total change.

For iCO<sub>2</sub> studies  $\text{CO}_2$  concentrations for the beginning and end of the time series were taken from the global annual values used in the most recent TRENDY simulations for the Global Carbon Project (Friedlingstein et al., 2019). For multi-site datasets we use the mean treatment  $\text{CO}_2$  values for eCO<sub>2</sub> experiments, and the mean start and end year for iCO<sub>2</sub> studies (primarily inventory studies). For meta-analysis studies that synthesised results from many different studies but did not report mean  $\text{CO}_2$  concentrations, we assume a value of 380 ppm for ambient  $\text{CO}_2$  conditions and 550 ppm for elevated  $\text{CO}_2$  conditions. To calculate uncertainties in  $\text{CO}_2$  we assume a 20 ppm in eCO<sub>2</sub> treatments and 5 ppm error in ambient  $\text{CO}_2$  treatments or historical iCO<sub>2</sub> studies (themes 2-4) to account for spatial variability from the global mean.

We report uncertainties as 95 % confidence intervals, converting from standard error of the mean by a factor of two. Where asymmetric confidence intervals were reported we take the mean of the absolute differences to estimate a single error term. 95 % confidence intervals for  $\beta$  were calculated using error propagation.

Where possible, for small net fluxes (i.e. where both input and output fluxes were of similar magnitude) we calculate  $\beta$  based on the standing stock of carbon. Where mean stocks ( $y_x$ ) and annual or per ppm changes were reported at source, we calculated the cumulative change ( $\Delta y$ ), calculated the initial value ( $y_a$ ) at  $\text{CO}_{2,a}$  from the mean stock minus half the change ( $y_a = y_x - \Delta y/2$ ). The value at  $\text{CO}_{2,e}$  was calculated as:  $y_a + \Delta y$ .

## Notes S3. Modelling leaf and canopy physiology

All modelling was done with the Multi-Assumption Architecture and Testbed (MAAT; Walker et al., 2018). Scripts to generate these data will be posted on Github (<https://github.com/walkeranthony/MAAT>). Leaf-scale photosynthesis was modelled following Farquhar et al. (1980) for C3 plants and Collatz et al., (1992) for C4 plants. Stomatal conductance was modelled following Dewar et al. (2018), which is very closely related to Medlyn et al. (2011).  $J_{\max}$  was related to  $V_{\text{cmax}}$  using the relationship commonly employed in many terrestrial biosphere models from Wullschlegel (1993).

Canopy-scale modelling was based on that in SDGVM (see Supporting Information Walker et al., 2017; Woodward and Lomas 2004) a 10-layer, multi-layer approach that includes sun and shade leaves and radiative transfer following Goudriaan (1977). Temperature scaling of  $V_{\text{cmax}}$  and  $J_{\max}$  was using the modified Arrhenius (Medlyn et al., 2002). Similar to SDGVM, a daily integral was achieved by assuming sine-wave scaling of photosynthetically active radiation at 20 points throughout the day with the peak scaled to a maximum daily value ( $2000 \mu\text{mol m}^{-2} \text{s}^{-1}$ ). Integration was through trapezoidal integration. A clear sky was assumed and solar zenith angle was assumed zero.

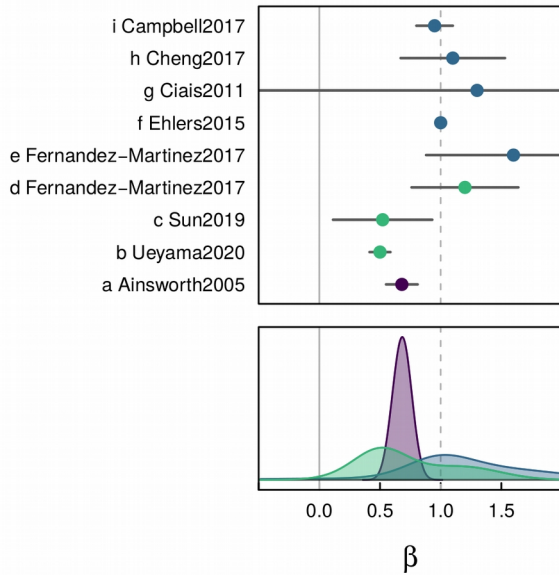
A 1000 member ensemble was run for each scale—instantaneous leaf, instantaneous canopy, and daily canopy. The ensemble comprised a factorial combination of 100 top-of-canopy  $V_{\text{cmax}}$  values (mean = 60, sd = 10) and 10 values of the  $J_{\max}$  to  $V_{\text{cmax}}$  slope (mean = 1.63, sd = 0.2). For the daily canopy simulations the 1000 member ensemble was run for a factorial combination of three levels of temperature (10, 15, 25 °C) and three levels of relative humidity (50, 70, 90 %).

For each ensemble member of these three scales,  $\beta_{\text{dir}}$  was calculated according to Eq. S3 (also Eq. 1 of the main text). Weighted mean  $\beta$ 's were calculated by weighting according to the absolute change in a variable with  $\text{CO}_2$ . Weighted 95 %iles were calculated using the weighted standard deviation multiplied by 2.

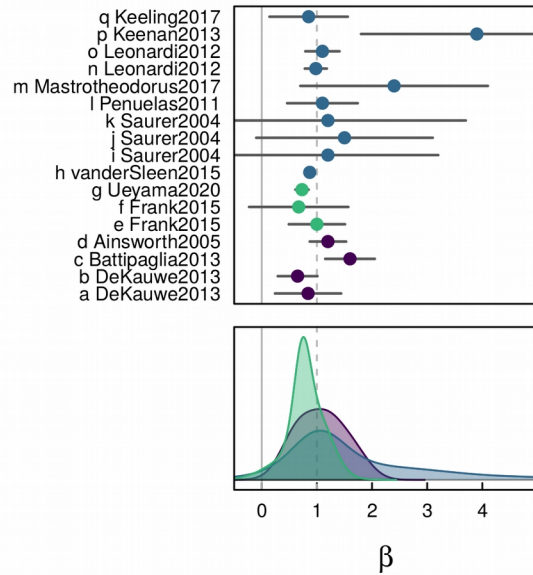
Table S1. Weighted  $\beta_{\text{dir}}$ 's (and 95 percentiles) from the model ensembles for  $A_{\text{net}}$ , light-saturated photosynthesis ( $A_c$ ), light-limited photosynthesis ( $A_i$ ), iWUE, and  $g_s$ .

Scale	$\Delta\text{CO}_2$	$\beta_{\text{dir}} A_{\text{net}}$	$\beta_{\text{dir}} A_c$	$\beta_{\text{dir}} A_i$	$\beta_{\text{dir}} \text{iWUE}$	$\beta_{\text{dir}} g_s$
Leaf	historical	0.86 (0.002)	0.86 (0.000)	0.31 (0.003)		-0.28 (0.002)
	future	0.70 (0.175)	0.74 (0.000)	0.23 (0.002)		-0.44 (0.25)
Canopy	historical	0.60 (0.2)	-	-	1.12 (0.01)	-0.56 (0.19)
	future	0.36 (0.2)	-	-	1.06 (0.01)	-0.75 (0.17)
Diurnal canopy	historical	0.60 (0.27)	-	-	1.07 (0.10)	-0.53 (0.17)
	future	0.46 (0.21)	-	-	1.03 (0.07)	-0.62 (0.15)

## GPP



## WUE



## BP

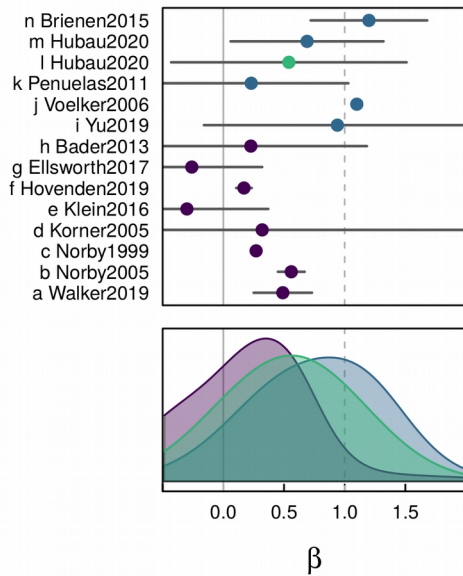
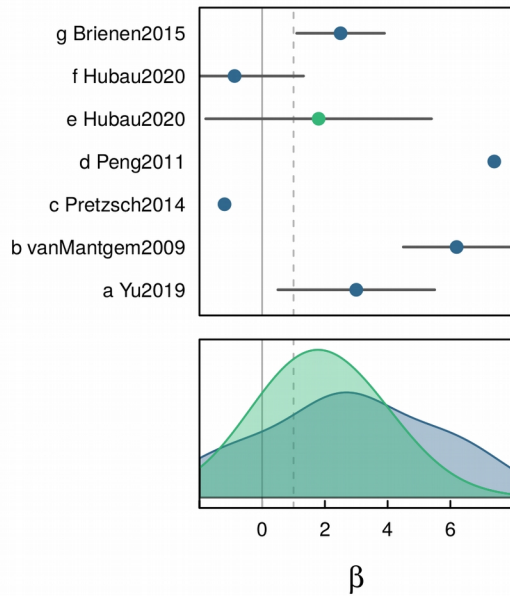
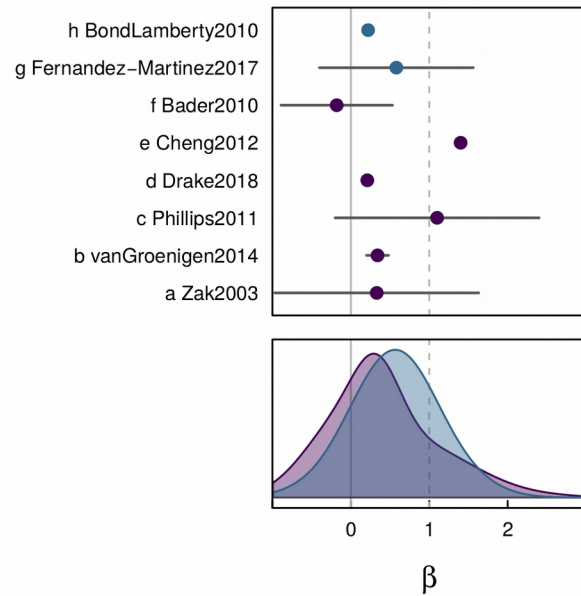


Figure S2.  $\beta$ 's with 95 % confidence intervals from Table 2 for GPP, WUE, BP. Data are organised by CO<sub>2</sub> response category—iCO<sub>2</sub> (blue), attribution to iCO<sub>2</sub> (green), and eCO<sub>2</sub> (purple). Also shown are PDFs of merged data for each CO<sub>2</sub> response category. PDFs are generated by drawing 1,000 random samples from the (assumed normal)  $\beta$  distributions for each study, and then combining all of these samples within each CO<sub>2</sub> response category. Studies with no CI were not included in the PDFs. In presenting variables together we have combined a number of related variables and at different scales, e.g. iWUE, WUE, and inherent WUE at scales from leaf, plant, ecosystem, to global are all presented on the WUE panel (see Table 2 for details).

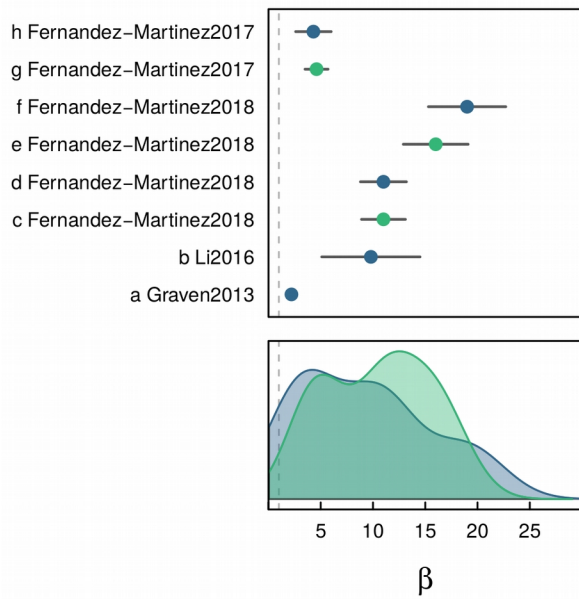
### k\_veg



### k\_soil



### NEP



### C\_veg\_increment

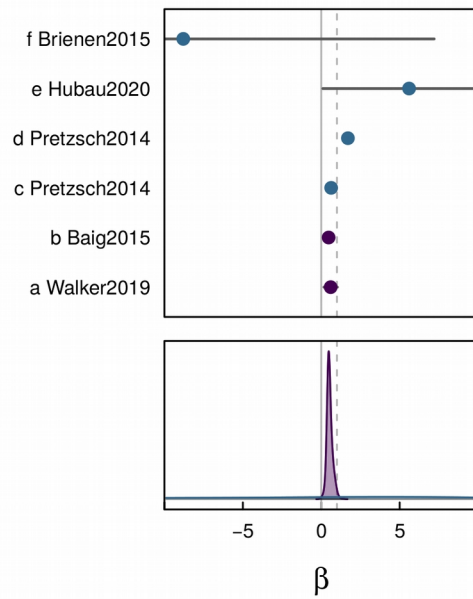
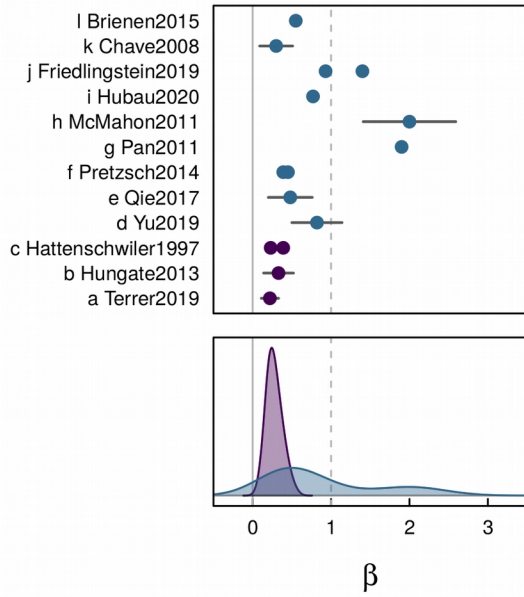


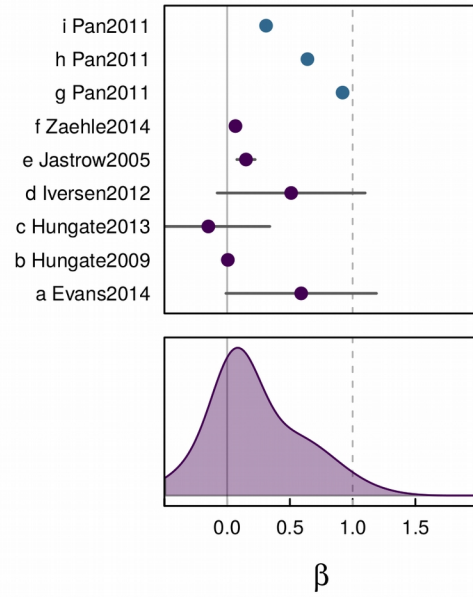
Figure S3.  $\beta$ 's with 95 % confidence intervals from Table 2 for  $k_{veg}$ ,  $k_{soil}$ , NEP, and  $C_{veg}$  increment. Details same as for Fig. S2.



### C\_veg



### C\_soil



### C\_eco

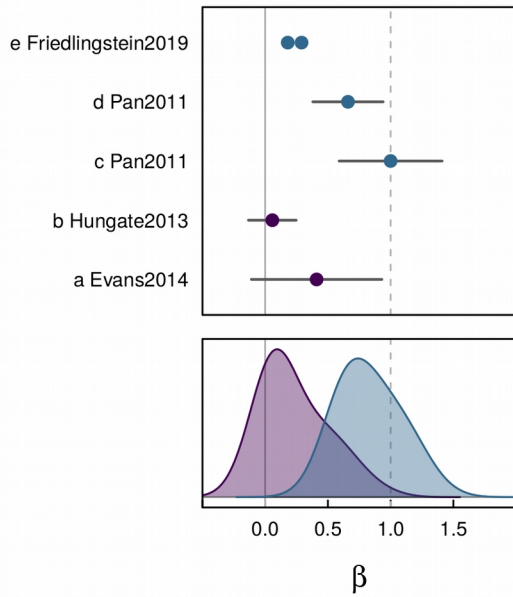


Figure S4.  $\beta$ 's with 95 % confidence intervals from Table 2 for  $C_{veg}$ ,  $C_{soil}$ , and  $C_{eco}$ . Details same as for Fig. S2.

## References

- Bacastow R, Keeling CK. 1973.** Atmospheric carbon dioxide and radiocarbon in the natural carbon cycle: II. Changes from A. D. 1700 to 2070 as deduced from a geochemical model. *Brookhaven Symposia in Biology*: 86–135.
- Collatz GJ, Ribas-Carbo M, Berry JA. 1992.** Coupled Photosynthesis-Stomatal Conductance Model for Leaves of C4 Plants. *Australian Journal of Plant Physiology* **19**: 519–538.
- Dewar R, Mauranen A, Mäkelä A, Hölttä T, Medlyn B, Vesala T. 2018.** New insights into the covariation of stomatal, mesophyll and hydraulic conductances from optimization models incorporating nonstomatal limitations to photosynthesis. *New Phytologist* **217**: 571–585.
- Farquhar GD, von Caemmerer S, Berry JA. 1980.** A biochemical model of photosynthetic CO<sub>2</sub> assimilation in leaves of C3 species. *Planta* **149**: 78–90.
- Friedlingstein P, Fung I, Holland E, John J, Brasseur G, Erickson D, Schimel D. 1995.** On the contribution of CO<sub>2</sub> fertilization to the missing biospheric sink. *Global Biogeochemical Cycles* **9**: 541–556.
- Friedlingstein P, Jones MW, O’Sullivan M, Andrew RM, Hauck J, Peters GP, Peters W, Pongratz J, Sitch S, Le Quéré C, et al. 2019.** Global Carbon Budget 2019. *Earth System Science Data* **11**: 1783–1838.
- Goudriaan J.** *Crop Micrometeorology: a Simulation Study*. Wageningen: Pudoc.
- Medlyn BE, Dreyer E, Ellsworth D, Forstreuter M, Harley PC, Kirschbaum MUF, Le Roux X, Montpied P, Strassmeyer J, Walcroft A, et al. 2002.** Temperature response of parameters of a biochemically based model of photosynthesis. II. A review of experimental data. *Plant Cell and Environment* **25**: 1167–1179.
- Picard G, Quegan S, Delbart N, Lomas MR, Le Toan T, Woodward FI. 2005.** Bud-burst modelling in Siberia and its impact on quantifying the carbon budget. *Global Change Biology* **11**: 2164–2176.
- Walker AP, Quaife T, van Bodegom PM, De Kauwe MG, Keenan TF, Joiner J, Lomas MR, MacBean N, Xu C, Yang X, et al. 2017.** The impact of alternative trait-scaling hypotheses for the maximum photosynthetic carboxylation rate (V<sub>cmax</sub>) on global gross primary production. *New Phytologist* **215**: 1370–1386.

**Walker AP, Ye M, Lu D, Kauwe MGD, Gu L, Medlyn BE, Rogers A, Serbin SP. 2018.** The multi-assumption architecture and testbed (MAAT v1.0): R code for generating ensembles with dynamic model structure and analysis of epistemic uncertainty from multiple sources. *Geoscientific Model Development* **11**: 3159–3185.

**Wullschleger SD. 1993.** Biochemical Limitations to Carbon Assimilation in C3 Plants—A Retrospective Analysis of the A/Ci Curves from 109 Species. *Journal of Experimental Botany* **44**: 907–920.